IOP Publishing Journal of Physics B: Atomic, Molecular and Optical Physics
J. Phys. B: At. Mol. Opt. Phys. **41** (2008) 205504 (7pp) doi:10.1088/0953-4075/41/20/205504

Quantum chessboards in the deuterium molecular ion

C R Calvert[1], T Birkeland[1,2], R B King[1], I D Williams[1] and J F McCann[1]

[1] School of Mathematics and Physics, Queen's University Belfast, Belfast BT7 1NN, UK
[2] Department of Mathematics, University of Bergen, N-5007 Bergen, Norway

E-mail: tore.birkeland@math.uib.no and c.calvert@qub.ac.uk

Received 13 June 2008, in final form 29 August 2008
Published 1 October 2008
Online at stacks.iop.org/JPhysB/41/205504

Abstract
We present a new algorithm for vibrational control in deuterium molecules that is feasible with current experimental technology. A pump mechanism is used for creating a coherent superposition of the D_2^+ vibrations. A short, intense infrared control pulse is applied after a chosen delay time to create selective interferences. A 'chessboard' pattern of states can be realized in which a set of even- or odd-numbered vibrational states can be selectively annihilated or enhanced. A technique is proposed for experimental realization and observation of this effect using 5 fs pulses of $\lambda = 790$ nm radiation, with intermediate intensity (5×10^{13} W cm^{-2}).

(Some figures in this article are in colour only in the electronic version)

1. Introduction

The ability to effect quantum control at the molecular level has many potential applications, such as control of reaction dynamics [1], selective electron localization [2] and applications in quantum information processing [3]. In order to characterize control mechanisms and afford useful comparison between experiment and theory the hydrogen diatomic (and its ion, H_2^+) is often used as a test-bed. Such fundamental systems are extremely useful for identifying basic physical mechanisms because of their simple electronic structure. The heavier isotopes of hydrogen, such as deuterium and deuterium hydride are equally accessible for quantum simulations and execute slower nuclear motion, thus deuterium (D_2) has become the preferred target for time-resolved studies.

In recent years, ultrashort laser pulses have been used to initiate, image [4, 5] and control [6, 7] the ultrafast dissociation of D_2^+ with the localization of the remaining bound electron also manipulated [2]. However, such control of fundamental molecular motion has not been limited to dissociation dynamics and progress has been made on studies of bound wavepacket motion, with control mediated by interactions occurring on timescales shorter than the motion itself. For example, coherent rotational motion in molecules can be induced and controlled [8, 9] in diatomic systems using intense-field pulses on sub-rotational timescales, with the mapping of rapidly rotating (hydrogenic) diatomics being recently achieved [10, 11].

Several proposals for coherent control of vibration in the deuterium molecular ion have been put forward, with similar underlying principles [3, 12, 13]. First an ultrashort 'pump' pulse can be used to induce strong-field tunnel ionization of a D_2 target on a sub-vibrational timescale (<25 fs) creating a D_2^+ nuclear wavepacket in a coherent superposition of vibrational states. Taking $t = 0$ as the moment of creation of the molecular ion state, the subsequent vibration can be given by the eigenfunction expansion

$$|\Psi(t)\rangle = \sum_n a_n |n\rangle \exp(-\mathrm{i}E_n t/\hbar), \tag{1}$$

where $\{|n\rangle\}$ denotes the set of vibrational eigenstates (discrete and continuous) of the molecular ion, and $\{E_n\}$ the corresponding energies. Each bound eigenstate component has an associated amplitude $\{a_n\}$ and evolves with frequency $\omega_n = E_n/\hbar$, where the population of each n state is $|a_n|^2$.

The evolution of the probability density is dictated by the beat frequencies $(\omega_n - \omega_{n'})$ between the eigenstates [14] with periods on the order of 20–30 fs for first-order beats $(n - n' = \pm 1)$. The anharmonicity of the potential means that the eigenstate components de-phase within a few vibration cycles [14]. The wavepacket will become spatially de-localized across the potential as time evolves but will re-form (to execute well-defined oscillations) whenever the phases

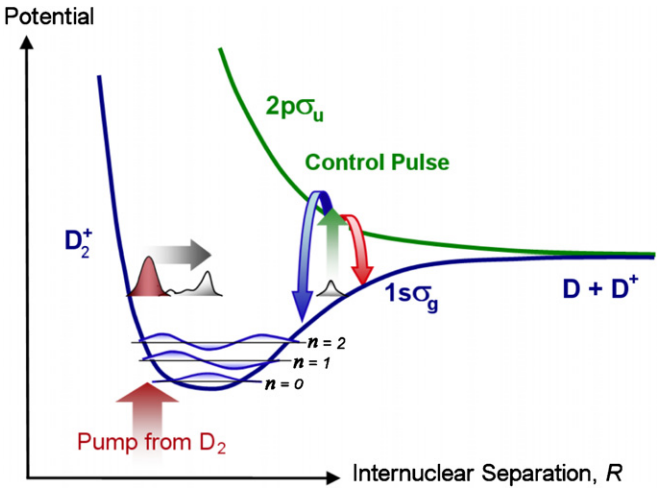

Figure 1. Schematic of vibrational control of D_2^+ (not to scale). An intense infrared pump laser interacts with the D_2 target in its ground vibrational state. The ionization process creates a coherent superposition of D_2^+ $1s\sigma_g$ vibrational states displaced from the minimum of the well. The wavepacket then oscillates, due to the displacement, and disperses, due to the anharmonicity of the D_2^+ state (silver arrow). The classical vibrational period (that is, for the centre of mass of the oscillation) is approximately 25 fs, while the vibrational states will fully de-phase and re-phase ('revive') after around 550 fs. The application of a secondary, control pulse initiates Raman transitions via the $2p\sigma_u$ surface creating Stokes (red arrow) and anti-Stokes (blue arrow) transitions.

of the components in (1) match. That is, when the beats have re-phased. This quantum 'revival' (at $t \sim 550$ fs) was recently measured [15, 16] and well reproduced by simulations [16, 17]. In these experiments rotational effects in the molecular ion were found to be negligible [16] due to the large range of vibrational states occupied, each with different rotational constants [18].

Suppose that, after some time τ in the wavepacket evolution, a secondary (control) pulse is used to alter the vibrational wavepacket. It has been shown that an infrared control pulse can produce an AC Stark effect that distorts the potential well (adiabatically) and hence modifies the wavepacket motion [12]. Depending on the wavepacket motion and position when the pulse is applied, a relative enhancement of lower vibrational populations may occur, i.e. vibrational cooling. While the adiabatic picture provides a useful physical interpretation, it does not fully explain the redistribution process.

To describe this, a Raman-type scheme has been proposed [3, 12, 13] where portions of the wavepacket may be transferred between the $1s\sigma_g$ (bound) and $2p\sigma_u$ (dissociative) potential, as seen in figure 1. In recent simulations, high-intensity pulses ($I \geqslant 10^{14}$ W cm^{-2}) have been used to enforce vibrational squeezing or 'quenching' into a specific state [13] or to create a coherent 2 (or 3) state wavepacket [3]. These studies were conducted with short delay times ($\tau <$ 100 fs), where the first-order vibrational beat components are de-phasing.

In this paper, we show that intermediate intensity ($I \sim 5 \times 10^{13}$ W cm^{-2}), few-cycle (5 fs) control pulses have important applications for coherent manipulation. We find a fascinating and hitherto unseen 'chessboard' pattern in the redistribution of the wavepacket population. In a different outcome to previous quenching/cooling studies, it is possible to selectively enhance almost *exclusively even* or *exclusively odd* numbered vibrational states. Thus the process relies on coherence in the energy domain, rather than wavepacket manipulation in the time domain. It is found that the mechanism of this process relies on constructive/destructive interference. This effect can be exploited at a fractional revival time to create strong-contrast interference patterns.

2. Simulations of vibrational control

In this paper, we simulate the control of a coherent D_2^+ vibrational wavepacket using a 5 fs, 5×10^{13} W cm^{-2} pulse. Referring to figure 1, an ultrashort 'pump pulse' (in this case provided by a Ti:Sapphire laser) interacts with the initial D_2 target in its ground vibrational state. The ionization process creates a coherent superposition of D_2^+ $1s\sigma_g$ vibrational states, as given in (1), displaced from the minimum of the potential well. The wavepacket then oscillates, due to the displacement, and disperses due to the anharmonicity of the D_2^+ state (silver arrow). The application of a secondary, control pulse initiates Raman transitions via the $2p\sigma_u$ surface (blue/red arrows), acting to redistribute the vibrational distribution of the wavepacket. This new vibrational distribution is studied as a function of the control pulse delay time, τ.

The initial D_2 target can be assumed to reside in the ground vibrational state of the $X^1\Sigma_g$ potential. In the Franck–Condon (FC) approximation, the ionization event would simply project this vibration function onto the manifold of vibrational states of the ion. Regarding this pump process, it is well known (see [19, 20], for example) that the tunnelling-ionization rate varies with bond length, even for the compact wavepacket presented by the D_2 ground vibrational state. This can modify the simple FC approximation that assumes the wavepacket is projected without modulation. We have carried out simulations using modulated wavepackets (displaced/broadened/skewed) as well as the FC wavepacket and find that the 'chessboard' interference effect we report here can be produced for each distribution. The FC approximation will be used here to demonstrate the 'chessboard' effect but it is not a necessary condition. A wavepacket with a range of populated vibrational states (such as those produced by intense infrared lasers) is sufficient. For initial distributions in a narrow range of vibrational states, the interference effects may not extend over as many states but will still occur. Indeed, for any experimental investigation the pump pulse parameters should be carefully chosen and compared to simulations for appropriate initial wavepacket conditions.

After the pump process, the FC wavepacket resides in the ground electronic state of the D_2^+ ion. At intermediate intensities, it is sufficient to solve the time-dependent equation for evolution on the two lowest potential curves ($1s\sigma_g$ and $2p\sigma_u$) within the Born–Oppenheimer approximation. With the infrared frequencies considered here, these two low-lying

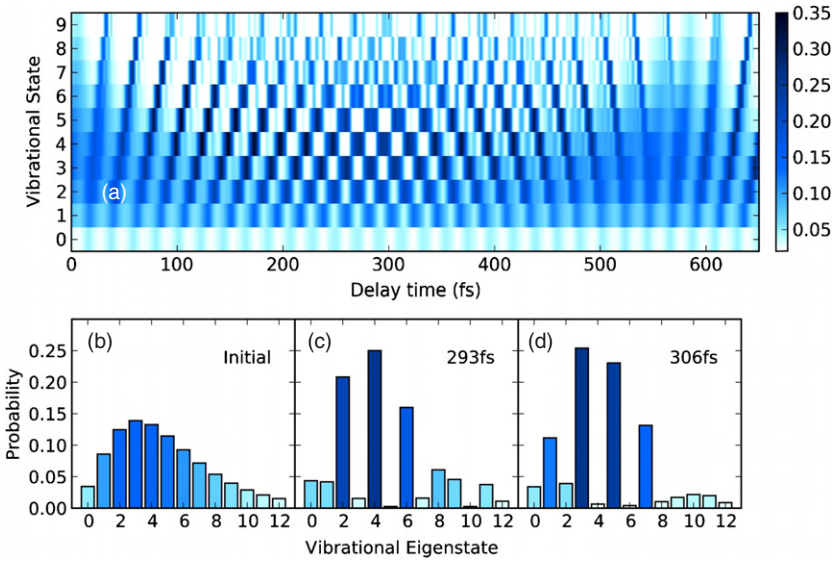

Figure 2. Vibrational distributions following a $\lambda = 790$ nm, $W = 5$ fs, $I = 5 \times 10^{13}$ W cm^{-2} control pulse, as a function of delay time τ. (a) The colour density represents the relative population of each level. (b) Initial probability distribution. For short delay times, $\tau < 100$ fs, and near the revival, $\tau \sim 550$ fs, the control pulse redistributes broadly with only slight enhancement in any single level. In contrast, the 'chessboard' pattern (centred around the fractional-revival $\tau \sim 300$ fs) shows an interference pattern in which even or odd numbered states are annihilated. For $\tau = 293$ fs and $\tau = 306$ fs, cuts through the colourmap are shown in (c) and (d).

levels need only be considered as higher lying electronic states are inaccessible. Thus the configuration space can be partitioned into g and u components. Then the Hamiltonian, H, can be partitioned into vibration, electronic motion and laser interaction as follows

$$H = T_R + H_e + V. \tag{2}$$

This has the matrix representation

$$H = \begin{pmatrix} T_R & 0 \\ 0 & T_R \end{pmatrix} + \begin{pmatrix} \varepsilon_g(R) & 0 \\ 0 & \varepsilon_u(R) \end{pmatrix} + \begin{pmatrix} 0 & F(t)d(R) \\ F(t)d(R) & 0 \end{pmatrix}, \tag{3}$$

where T_R is the vibrational kinetic energy operator, $\varepsilon_g(R)$ and $\varepsilon_u(R)$ are the potential energy curves for the $1s\sigma_g$ and $2p\sigma_u$ electronic states respectively, and $d(R)$ is the dipole moment between these states [21]. The external electric field $F(t)$ is created by a Ti:Sapphire laser with $\lambda = 790$ nm, modulated by a Gaussian profile centred at $t = \tau$ (the delay time), with full-width-half-maximum of W (the duration), that is

$$F(t) = F_0 \cos(\omega(t-\tau)) \exp\{-2\ln 2(t-\tau)^2/W^2\}. \tag{4}$$

The (cycle-average) intensity, I, of the pulse is related to the electric-field amplitude, F_0, by the formula, $I = \frac{1}{2}\epsilon_0 c F_0^2$. The evolution of the equations is computed by a symmetric, split-step algorithm [22]

$$\begin{aligned} |\psi(t+\Delta t)\rangle = {} & \exp(-\mathrm{i}T_R\Delta t/2)\exp(-\mathrm{i}H_e\Delta t/2) \\ & \times \exp(-\mathrm{i}V(t)\Delta t)\exp(-\mathrm{i}H_e\Delta t/2) \\ & \times \exp(-\mathrm{i}T_R\Delta t/2)|\psi(t)\rangle + O(\Delta t^2). \end{aligned} \tag{5}$$

The error term in this expression arises partly from the splitting (factorization) and from assuming that the Hamiltonian changes slowly over the time step (time-ordering error). In practice, the time-step Δt is chosen as sufficiently small so that, $\Delta t(\partial H/\partial t) \ll H$.

The splitting and the use of a uniform grid means the highly efficient fast Fourier transform [23] can be employed. The electronic coupling term V is diagonal in the radial dimension, and a diagonalization of the 2×2 submatrix gives an efficient scheme for propagation:

$$\begin{aligned} \exp\left[-\mathrm{i}\Delta t \begin{pmatrix} 0 & F(t)d(R) \\ F(t)d(R) & 0 \end{pmatrix}\right] = {} & \frac{1}{2}\begin{pmatrix} \mathbb{1} & \mathbb{1} \\ -\mathbb{1} & \mathbb{1} \end{pmatrix} \\ & \times \begin{pmatrix} \exp(-\mathrm{i}F(t)d(R)\Delta t) & 0 \\ 0 & \exp(\mathrm{i}F(t)d(R)\Delta t) \end{pmatrix} \\ & \times \begin{pmatrix} \mathbb{1} & -\mathbb{1} \\ \mathbb{1} & \mathbb{1} \end{pmatrix}, \end{aligned} \tag{6}$$

where $\mathbb{1}$ is the unit matrix. The vibrational populations are projections of the g-state wavepacket on the manifold, $\{|n\rangle\}$, while the dissociation yield will be defined by the population in the u state along with the g-state continuum.

3. The chessboard

The vibrational populations, following the application of a short control pulse ($W = 5$ fs), with $I = 5 \times 10^{13}$ W cm^{-2}, were calculated for a range of delay times 0 fs $\leqslant \tau \leqslant$ 650 fs. The results are presented in figure 2. The colour density in figure 2(a) represents the final population of a vibrational level with respect to the control pulse delay. The distributions resulting from $\tau = 293$ fs and $\tau = 306$ fs are extracted from figure 2(a) and displayed as the bar charts 2(c) and 2(d), respectively. The initial probability distribution is shown in figure 2(b).

In previous studies, the modulations in population had been attributed to the classical vibrational period of each level

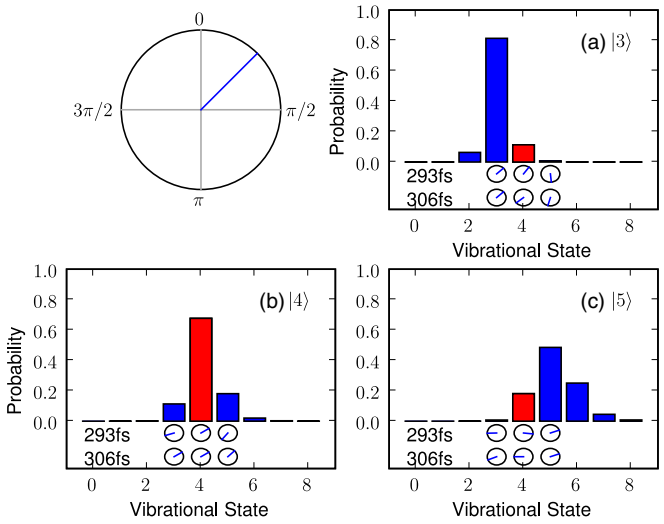

Figure 3. Vibrational transfer starting from (a) $n = 3$, (b) $n = 4$ and (c) $n = 5$ by a 5 fs, $\lambda = 790$ nm, $I = 5 \times 10^{13}$ W cm^{-2} control pulse. The bar charts represent the probabilities $|a_n|^2$ while the clocks display the phase of the coefficients a_n after the pulse for $\tau = 293$ fs and $\tau = 306$ fs. The distributions are concentrated around the initial state, while the initial state is phase-advanced. This illustrates that a coherent sum of the final distributions will depend strongly on τ. For the reader's convenience, the contributions into $|4\rangle$ are highlighted in red, see the text for details.

[13]. Here a description for the mechanism will be given in terms of interference processes in the energy domain regulated by the beat frequencies.

For short delays ($\tau < 50$ fs) the anharmonic correction is small, and dephasing is not significant. Under such conditions, the control pulse spreads the population evenly with only slight enhancements/deficits. In the region $\tau \sim 100$ fs, enhancement is concentrated on a specific level (e.g. $n = 4$ at $\tau = 100$ fs). These effects are repeated around the wavepacket revival (∼550 fs), where the wavepacket begins to re-form and then de-phase again. Higher-intensity control pulses can be used to optimize state-selective control [3, 13] and drive population towards one or more specific levels.

The most striking feature of figure 2(a) is the alternating light and dark squares, suggestive of a 'chessboard' pattern, centred around $\tau \sim 300$ fs. At this fractional revival time, the even-numbered vibrational states will be in phase with each other but in anti-phase with the 'odd' states. This phase relationship can be exploited to produce interference effects. The effect is illustrated in figure 2(c), where at $\tau = 293$ fs the non-negligible populations are *exclusively* in *even* numbered states. Likewise at $\tau = 306$ fs only *odd* numbered states are populated, with $n = 1, 3, 5, 7$ strongly favoured.

The effect can be understood by the destructive/constructive interference between nearest-neighbour states. Suppose we consider the effect of the pulse on isolated states $n = 3, 4, 5$, separately. In figure 3 the final amplitudes and phases for each state are illustrated by bar charts and clocks respectively. The clocks display the phase shifts for the wavepacket population moved into each level, with the relative phase shift defined with respect to the expected phase for an unperturbed state. All clocks will remain at 12 o'clock in the absence of any perturbation. In each case, starting with a single vibrational state, the final probability distribution is independent of τ. We also note a selection rule favouring neighbouring levels. To illustrate this, let us focus on the state $n = 4$. For the reader's convenience, the bar charts showing the contributions into $|4\rangle$ are highlighted in red in figure 3. At the delay time $\tau = 293$ fs, the contributions to $|4\rangle$ from all three initial states have roughly the same phase, i.e. they interfere constructively. In contrast, at $\tau = 306$ fs, the contributions from $|3\rangle$ and $|5\rangle$ are almost opposite to the contribution from $|4\rangle$, giving a destructive interference. For the final population in $|5\rangle$, the situation is opposite yielding destructive and constructive interference for $\tau = 293$ fs and 306 fs respectively. This pattern is repeated so that even numbered states get enhanced and odd numbered states get quenched for $\tau = 293$ fs, and vice versa for $\tau = 306$ fs giving rise to the chessboard effect seen in figure 2.

Some previous work on wavepacket engineering focussed on manipulation in configuration space. The chessboard is an effect that pertains to engineering in the energy dimension. We note that, although the chessboard state is highly regular in energy space, the wavepacket in configuration space is still quite irregular as time progresses.

4. Model

A simple mathematical model of the interference can be obtained from perturbation theory. As a preliminary comment, the hierarchy of timescales in this system is worth noting, from the fast electronic motion to the medium-speed optical field, through to the comparatively 'slow' vibrational motion. The 'electronic time' is of the order of the dissociation energy of the molecule, with an associated angular frequency: $\sim 25 \times 10^{15}$ rad s^{-1} ≈ 0.6 au, while the optical cycle time is $\omega_{\rm opt} \sim 2.4 \times 10^{15}$ rad s^{-1} ≈ 0.06 au, and finally the vibration time $\omega_e \sim 0.3 \times 10^{15}$ rad s^{-1} ≈ 0.007 au. Consequently the pulse interaction is sudden compared to the vibrational timescale, but adiabatic in the context of the electronic motion.

The effect of a laser pulse after a delay τ can now be considered. A simple mathematical model can be constructed where the modulated sinusoidal signal of the laser pulse is considered as a sequence of alternating square waveforms. The expansion

$$|\psi(t)\rangle = \sum_{\gamma,n} a_{\gamma,n}(t)\, \mathrm{e}^{-\mathrm{i}E_{\gamma,n}t}|\gamma, n\rangle, \tag{7}$$

can be proposed as the solution to

$$\mathrm{i}\frac{\partial}{\partial t}|\psi(t)\rangle = H(t)|\psi(t)\rangle, \tag{8}$$

where $\gamma \in \{g, u\}$ is the electronic state with corresponding vibration state (bound and/or dissociative) n. Equation (8) can be written as a set of integral equations ($t \geqslant t_0$):

$$a_{\gamma,n}(t) = a_{\gamma,n}(t_0) - \mathrm{i}\sum_{\gamma',n'}\int_{t_0}^{t} \mathrm{d}t' a_{\gamma',n'}(t') V_{\gamma,n;\gamma',n'}(t') \times \exp[\mathrm{i}\Delta_{\gamma,n;\gamma',n'}t'], \tag{9}$$

where $\Delta_{\gamma,n;\gamma',n'} = E_{\gamma,n} - E_{\gamma',n'}$ and the coupling potential V is expanded in the basis set in equation (7). In the two-state approximation the only non-zero element has the form

$$V_{g,n;u,k}(t') = V_{u,k;g,n}(t') = F(t)\langle k|d(R)|n\rangle, \tag{10}$$

where $|k\rangle$ is an energy-normalized continuum function of the u-state, with wavenumber k, and $|n\rangle$, is a vibrational eigenstate (bound or continuum) of the g-well.

The photon energy (∼0.06 au in this case) is below the single-photon resonant dissociation for all states of the g potential that are shown in figure 2, and for laser intensities lower than 10^{14} W cm^{-2}, the upper electronic level u acts as a virtual state. The expansion coefficients of (7) of the g-state can then be calculated to second-order accuracy:

$$\begin{aligned} a_{g,n}(\tau + W) = a_{g,n}(0) + (-\mathrm{i})^2 \sum_{k,n'} \int_{\tau}^{\tau+W} \mathrm{d}t' \\ \times \exp[\mathrm{i}\Delta_{g,n;u,k}t']V_{g,n;u,k}(t') \\ \times \int_{\tau}^{t'} \mathrm{d}t'' \exp[\mathrm{i}\Delta_{u,k;g,n'}t'']V_{u,k;g,n'}(t')a_{g,n'}(0). \end{aligned} \tag{11}$$

For simplicity, consider the pulse to be applied impulsively after a delay τ, for a duration W' (corresponding to half an optical cycle), with amplitude F_0. A further simplification can now be made in the summation over the intermediate states. The 'closure approximation' replaces the spectrum of intermediate energies by a constant, $E_{u,k} = \bar{E}$, representative of the dominant (resonant) channels. In fact the choice of $\bar{E}$ can be used as a free parameter if desired, but it must lie in the continuum. In the spirit of the approximation, we choose $\bar{E}$ as the threshold of dissociation in the u state also reflecting the enhanced density of states at threshold. Then taking this as the reference point for the zero of energy, we simply set $\bar{E} = 0$. The closure (completeness) relation can then be applied so that

$$\sum_k \langle n|d(R)|k\rangle\langle k|d(R)|n'\rangle = \langle n|d^2(R)|n'\rangle \equiv d^2_{n,n'}. \tag{12}$$

The index g may now be dropped for convenience and we have

$$\begin{aligned} a_n(\tau + W') = a_n(0) \\ - \sum_{n'} a_{n'}(0)d^2_{n,n'}F_0^2 \int_{\tau}^{\tau+W'} \mathrm{d}t' \, \mathrm{e}^{\mathrm{i}E_n t'} \int_{\tau}^{t'} \mathrm{d}t'' \, \mathrm{e}^{-\mathrm{i}E_{n'}t''}, \end{aligned} \tag{13}$$

and this may be evaluated without further approximation.

As seen in figure 4, the matrix element $d^2_{n,n''}$ provides an approximate selection rule: $n' = n, n \pm 1$, so that the expression can be reduced even further. Moreover, since $E_n W' \gg 1$, the solution can then be expressed in the simple form:

$$\begin{aligned} a_n(\tau + W') \approx a_n(0)\,(1 - \mathrm{i}\kappa_{nn}) - \mathrm{i}\kappa_{n,n-1}a_{n-1}(0)\,\mathrm{e}^{\mathrm{i}(E_n - E_{n-1})\tau} \\ - \mathrm{i}\kappa_{n,n+1}a_{n+1}(0)\,\mathrm{e}^{\mathrm{i}(E_n - E_{n+1})\tau}, \end{aligned} \tag{14}$$

where,

$$\kappa_{n,n'} = \left(\frac{F_0^2 d^2_{n,n'}}{E_{n'}}\right)\left(\frac{\exp[\mathrm{i}(E_n - E_{n'})W'] - 1}{\mathrm{i}(E_n - E_{n'})}\right). \tag{15}$$

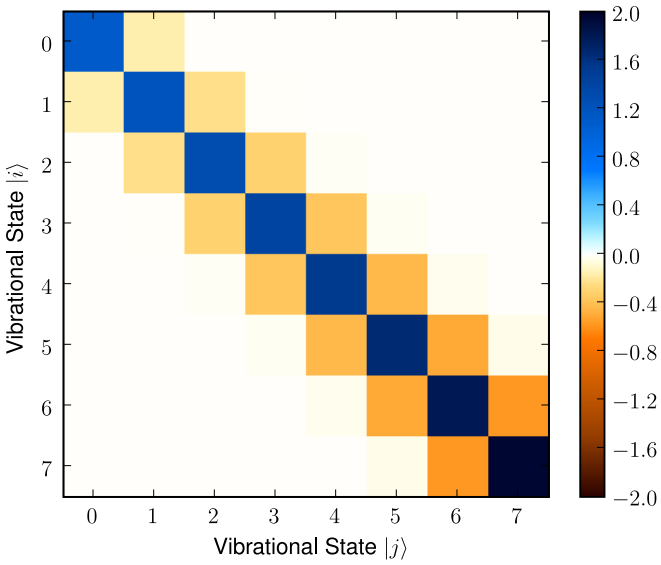

Figure 4. Second-order coupling strength between vibrational eigenstates during the laser pulse $(d^2)_{ij}$. Note the rapid decrease in coupling strength as $|i - j|$ grows leading to an approximate selection rule $i - j \in \{-1, 0, 1\}$ for intermediate fields. This arises from the linear form of the function $d(R)$. Also note that the coupling strength increases with vibrational levels, giving a rise to slight heating, i.e. propensity towards higher vibrational levels.

In the case of a very short impulse, corresponding to a half-cycle, $(E_n - E_{n-1})W' \ll 1$, and

$$\kappa_{n,n'} \approx \left(\frac{F_0^2 W'}{E_{n'}}\right) d^2_{n,n'}. \tag{16}$$

The term $\kappa_{n,n}$ simply reflects the change in phase due to the quadratic Stark effect. Since this is a second-order effect, the sign of F_0 has no consequence, and $\kappa_{n,n} < 0$, and hence there is a phase advance. This is illustrated in figure 3 where the parent state is phase shifted forward, with the excited state $n = 5$ more advanced than the lower-energy state $n = 3$, in agreement with this expression for the energy dependence. We note that, in this model, $\kappa_{n,n'}$ is not sensitive to the sign of F_0, that is, to the carrier envelope phase. Thus a sequence of alternating half-cycles creates the same effect as a full-wave rectified pulse.

Consider the effect of one half-cycle. The equations above have the simple explanation that $a_n(\tau + W')$ is created by an interference pattern with its immediate neighbours. This pattern can be regular if the terms on the right-hand side are coherent. In order to create strong destructive interference, the terms $(\kappa_{n,n-1}a_{n-1}(0) + \kappa_{n,n+1}a_{n+1}(0))$ must be approximately the same size as the remaining term $a_n(0)(1 - \kappa_{n,n})$ for $n \in 2, \ldots, 6$. This gives an optimal value of F_0 and W'. Next, the phases of the two interference terms must be equal, which implies the condition (for all n):

$$(E_n - E_{n-1})\tau = -(E_{n+1} - E_n)\tau, \qquad \mathrm{mod}(2\pi). \tag{17}$$

A rough estimate of this condition on τ, can be made by the anharmonic expansion, $E_n \approx -D_e + \hbar\omega_e\left(n + \frac{1}{2}\right) - \hbar\omega_e x_e\left(n + \frac{1}{2}\right)^2$, where D_e is the dissociation energy. This is satisfied during the fractional revival around $\tau \approx \pi/(2\omega_e x_e) \sim$

280 fs. Finally, these terms must be out of phase with a_n to create destructive interference. The Stark effect (14) creates a phase shift, $-\kappa_{n,n}$, for the state n. Thus in order to get destructive interference, the requirement is then

$$\kappa_{n,n} = (E_n - E_{n-1})\tau + \pi/2, \qquad \mathrm{mod}(2\pi). \tag{18}$$

If destructive interference occurs for even n, then according to equation (17), constructive interference will be observed for odd n. Furthermore, if destructive interference is observed for a state at $\tau = \tau_0$, constructive interference will be observed for $\tau = \tau_0 + \pi/\omega_e \approx \tau_0 + 11$ fs. This is a qualitative explanation, and is limited by the crudeness of the closure approximation. Further, the assumptions we make for the pulse are simple. Nevertheless, it appears that this simple model explains the main features that we observe in the numerical simulations.

5. Proposed experimental technique for observing the chessboard

Having simulated the chessboard pattern and explained the underlying mechanism, attention can be turned to techniques for experimental observation of this fascinating effect. In recent experiments [15, 16], coherent vibrational wavepacket motion in D_2^+ has been initiated and imaged in a pump-probe configuration using short intense-field pulses. In these studies the vibrational wavepacket motion, and notably the vibrational revival, has been imaged by using a probe pulse to enforce photodissociation or Coulomb explosion of the vibrating molecule across a range of probe delay times.

Fourier analysis of the fragmentation yield can return a measure of both the temporal and spatial nature of the wavepacket motion, which can ultimately lead to full characterization of the molecular motion [24]. In particular, the beat frequencies that dictate the motion of the probability density can be extracted from the photodissociation signal.

Thus it may be possible to conduct a pump-control-probe experiment where a new coherent vibrational distribution (created at a specific control pulse delay time) may be monitored by recording the total dissociation yield as a function of probe delay time (τ') with subsequent spectral analysis of the signal.

It is important that for modelling any such experiment, the pump process is well characterized. For pulse intensities of $\sim 1 \times 10^{14}$ W cm^{-2} the R-dependence (see [25] and references therein) of the pump process has been considered in recent studies of D_2^+ wavepackets [13, 24, 26], and indeed in some recent experiments [15] the results appear to deviate from an FC wavepacket. It is noted here that the R-dependence of the pump process is sensitive to pulse intensity [27] and, as pulse intensity increases, the resulting ion may tend towards an FC distribution [27]. However, if the intensity is set too high there is a probability that direct fragmentation of the D_2 target may occur in the initial pump pulse, clouding the detection of any bound wavepacket dynamics from the control or probe pulse interactions.

At this point, it is instructive to observe that in other recent experiments [16, 17] with pump pulses (λ = 790 nm) of duration 10–15 fs, and intensities of 5–8 $\times$ 10^{14} W cm^{-2} the wavepacket dynamics are in fact well reproduced by Franck–Condon simulations. In these experiments the problem of direct D_2 fragmentation from an intense pump pulse is overcome by orienting the pump pulse polarization perpendicular to the detection axis, ensuring that any direct fragmentation arising from this pulse goes undetected.

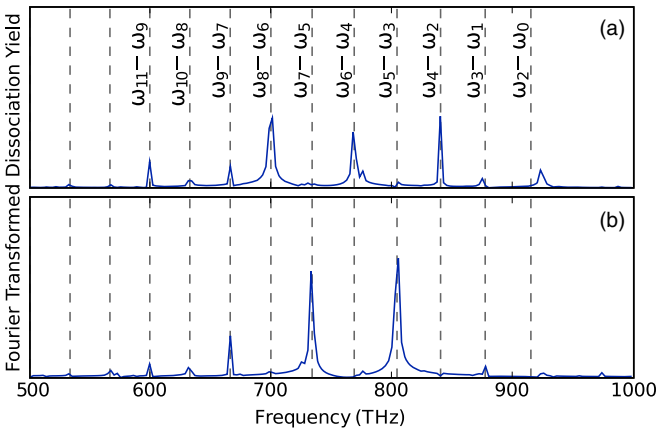

Figure 5. Spectral density for the dissociation yields correlation function. The coherent D_2^+ wavepacket is controlled by a 5 fs, $\lambda = 790$ nm, $I = 5 \times 10^{13}$ W cm^{-2} pulse at $\tau = 293$ fs and $\tau = 306$ fs for plots (a) and (b) respectively. The probe pulse is, $\lambda = 790$ nm, $I = 4 \times 10^{14}$ W cm^{-2}, duration 5 fs. Fourier analysis of the dissociation signal returns the vibrational beats $\omega_{n+2} - \omega_n$ present in the wavepacket motion in each case. The probe delay time ranges from 310 fs to 4000 fs. A shorter range of times, 310 fs to 1000 fs for example, gives similar features. In this case the peaks are broadened but still well resolved.

In this context, the proposed experimental technique for identifying the chessboard effect has been simulated for an FC wavepacket. This was done by fixing the control pulse at a desired τ value, and introducing an intense probe pulse (5 fs duration, $I = 4 \times 10^{14}$ W cm^{-2}) at a variable delay time τ'. The dissociation yield was deduced by subtracting the remaining bound wavepacket population from the initial norm of the wavepacket. The Fourier transform (energy spectral density) of the dissociation signal is shown in figure 5 for control delay times of (a) $\tau = 293$ fs and (b) $\tau = 306$ fs. The calculations represent the signal correlation over very long times (4000 fs). We have performed the same analysis over a much shorter time (1000 fs) and, although the features are broadened, the signatures are still clearly visible.

The individual states in the vibrational distribution are not resolved in isolation but rather the peaks in figure 5(a) correspond to the beat frequencies between even states. These are notably absent in figure 5(b), where only the odd numbered eigenstate beat frequencies are observed, in keeping with the expected vibrational distributions (from figure 2). The amplitude of the beat $\omega_{n+2} - \omega_n$ in the wavepacket motion is given by $|a_n a_{n+2}|$. The Fourier transform technique will not extract the absolute population values, $|a_n a_{n+2}|$ but rather, will provide insight into which states are significantly populated. This is a useful technique for experimentally identifying the preferential creation of either *even* or *odd* numbered states. It should be noted however that periods of the $\omega_{n+2} - \omega_n$ beats are

typically 10–12 fs and thus for any experimental verification, it is imperative that pulses as short as 5 fs are used.

In principle, this technique using the photodissociation signal could be a useful method for identifying the main components of the wavepacket, and with state-of-the-art pulses now available for durations less than 10 fs, this should be achievable in the laboratory in the not too distant future. Indeed, with continuing advances in intense-field laser-pulse experiments, such an even (or odd) state wavepacket (evolving with ∼12 fs oscillations) may even be characterized by using a high-intensity probe pulse and a very recently reported 'time-series analysis' of the Coulomb explosion signal [26], where full reconstruction of the wavepacket has been proposed.

6. Conclusion

In this paper, the application of an intermediate intensity (5×10^{13} W cm^{-2}) few-cycle (5 fs) pulse to control a coherent vibrational wavepacket in D_2^+ has been investigated. The redistribution of vibrational levels proceeds by a Raman transfer between near-neighbour levels. This creates interferences such that it is possible to produce strong-contrast fringes of the even/odd numbered vibrational levels. The effect is a property of the molecular ion and does not require a highly-selective ionization process. All that is required is that a band of vibration states is populated. Simulations using the Franck–Condon approximation are shown for illustration but this is not a necessary condition.

The 'chessboard' pattern that emerges around $\tau \sim$ 275–300 fs provides a pathway for creating almost *exclusively even* or *exclusively odd* numbered vibrational distributions in a coherent wavepacket. Thus the process relies on coherence in the energy domain, rather than wavepacket manipulation in the time domain. The subsequent propagation of such a created wavepacket may be probed via photodissociation and here it has been shown that spectral analysis of the dissociation data may serve to identify the populated states. This provides a pathway for using currently available ultrashort laser pulse technology to investigate this 'chessboard' effect.

Acknowledgments

CRC and RBK wish to acknowledge funding from the Department of Employment and Learning (NI).

References

[1] Mokhtari A, Cong P, Herek J L and Zewail A H 1990 *Nature* **348** 225
[2] Kling M F *et al* 2006 *Science* **312** 246–8
[3] Murphy D S, McKenna J, Calvert C R, Williams I D and McCann J F 2007 *New J. Phys.* **9** 260
[4] Trump C, Rottke H and Sandner W 1999 *Phys. Rev.* A **59** 2858
[5] Ergler Th, Rudenko A, Feuerstein B, Zrost K, Schröter C D, Moshammer R and Ullrich J 2005 *Phys. Rev. Lett.* **95** 093001
[6] Murphy D S *et al* 2007 *J. Phys. B: At. Mol. Opt. Phys.* **40** S359
[7] Niikura H, Villeneuve D M and Corkum P B 2006 *Phys. Rev.* A **73** 021402
[8] Lee K F, Shapiro E A, Villeneuve D M and Corkum P B 2006 *Phys. Rev.* A **73** 033403
[9] Fleischer S, Averbukh I Sh and Prior Y 2008 *J. Phys. B: At. Mol. Opt. Phys.* **41** 074018
[10] Lee K F, Légare F, Villeneuve D M and Corkum P B 2006 *J. Phys. B: At. Mol. Opt. Phys.* **39** 4081
[11] Bryan W A, English E M L, McKenna J, Wood J, Calvert C R, Torres R, Turcu I C E, Collier J L, Williams I D and Newell W R 2007 *Phys. Rev.* A **76** 023414
[12] Niikura H, Villeneuve D M and Corkum P B 2004 *Phys. Rev. Lett.* **92** 133002
[13] Niederhausen T and Thumm U 2008 *Phys. Rev.* A **77** 013407
[14] Feuerstein B and Thumm U 2003 *Phys. Rev.* A **67** 063408
[15] Ergler Th, Rudenko A, Feuerstein B, Zrost K, Schröter C D, Moshammer R and Ullrich J 2006 *Phys. Rev. Lett.* **97** 193001
[16] Bryan W A *et al* 2007 *Phys. Rev.* A **76** 053402
[17] McKenna J *et al* 2007 *J. Mod. Opt.* **54** 7 1127
[18] Bocharova I A, Mashiko H, Magrakvelidze M, Ray D, Ranitovic P, Cocke C L and Litvinyuk I V 2008 *Phys. Rev.* A **77** 053407
[19] Saenz A 2000 *J. Phys. B: At. Mol. Opt. Phys.* **33** 4365–72
[20] Posthumus J H and McCann J F 2001 *Molecules and Clusters in Intense Laser Fields* ed J H Posthumus (Cambridge: Cambridge University Press)
[21] Bates D R 1951 *J. Chem. Phys.* **19** 1122
[22] Hermann M R and Fleck J A 1988 *Phys. Rev.* A **38** 6000
[23] Frigo M and Johnson S G 2005 *Proc. IEEE* **93** 216
[24] Feuerstein B, Ergler Th, Rudenko A, Zrost K, Schrter C D, Moshammer C D, Ullrich J, Niederhausen T and Thumm U 2007 *Phys. Rev. Lett.* **99** 153002
[25] Awasthi M and Saenz A 2006 *J. Phys. B: At. Mol. Opt. Phys.* **39** S389
[26] Thumm U, Niederhausen T and Feuerstein B 2008 *Phys. Rev.* A **77** 063401
[27] Urbain X, Fabre B, Staicu-Casagrande E M, de Ruette N, Andrianarijaona V M, Jureta J, Posthumus J H, Saenz A, Baldit E and Cornaggia C 2004 *Phys. Rev. Lett.* **92** 163004